Controller-Hardware-in-the-Loop Investigations for a Partly Superconducting Medium-Speed Wind Turbine Generator Prototype

Nick Thönelt[1]*, Benedikt Schmitz-Rode[1], Nils Rickertsen[1], Lukas Stefanski[1], Marc Hiller[1]
1 Elektrotechnisches Institut (ETI), Karlsruhe Institute of Technology (KIT), Karlsruhe, Germany
*nick.thoenelt@kit.edu

***Abstract*—This paper presents a comprehensive Controller-Hardware-in-the-Loop (CHiL) investigation for a multi-megawatt-scale, partly superconducting, medium-speed wind turbine generator prototype. The CHiL approach is employed to safely and efficiently test the generator's sophisticated control system by interfacing a real controller with a high-fidelity, real-time simulation of the generator and its power converter. The generator design incorporates a superconducting rotor winding to reduce the overall size and mass for large-scale offshore wind applications while featuring high efficiency. The core of the CHiL real-time model is a highly non-linear, flux-based representation of the electrically excited synchronous machine. A key aspect is the critical importance of modeling the coupled generator-converter system for partly superconducting generators. Previous findings within the scope of the presented project demonstrate that the non-sinusoidal voltage and current from the converter feeding can introduce significant eddy current losses, potentially dominating thermal loads in the cryogenic rotor parts compared to ideal sine-wave operation. This work is a crucial step in the development of future control strategies for a megawatt-scale prototype, which is currently under construction.**

***Index Terms*—Hardware-in-the-loop, Real time processing, Wind power generation, Synchronous machines, Power electronics.**

I. Introduction

The transition toward a decarbonized energy system is driving the development of larger and more powerful wind turbines. For multi-megawatt offshore wind applications, the logistical and economic challenges associated with size and mass, particularly for direct-drive generators, are substantial. Superconducting technology offers a promising solution by enabling high generator power densities and eliminating resistive losses, thereby reducing the generator's footprint and weight while achieving high efficiency. This paper considers the use of a partly superconducting synchronous machine with a conventional stator and a superconducting rotor winding, developed within a publicly funded project aimed at creating a megawatt-scale prototype by 2026 [1]- [2].

The development of such an innovative generator and its control system requires a robust and safe testing environment. Full-scale prototype testing is costly and includes extensive preparation, especially because of the high power rating and cryogenic system of this particular machine. Controller-Hardware-in-the-Loop (CHiL) tests provide an ideal environment, allowing the actual physical controller to be tested against a real-time, high-fidelity numerical model of the generator and its power converter. This method facilitates comprehensive testing under a wide range of operating conditions, including nominal operation, transient load changes and various fault scenarios, without endangering the prototype and without computationally intensive simulations [3]. This paper extends previous work on the implementation of flux-based machine models on rapid prototyping systems and applies this methodology to the investigation of the partly superconducting generator prototype. The main focus of the presented study is on the interactions between the power converter feeding the machine and the resulting spectral analysis of stator currents to estimate eddy current losses in the cryogenic rotor parts.

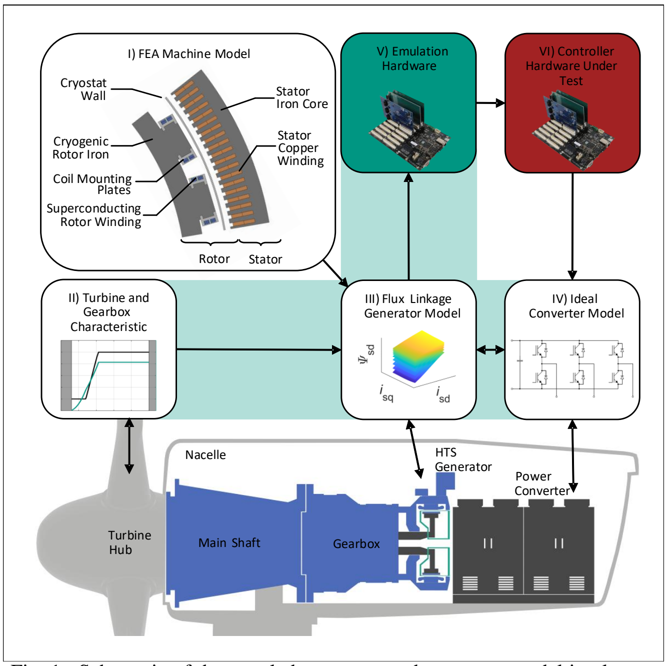

Fig. 1. Schematic of the coupled generator and converter model implemented on the CHiL system

II. System Architecture and Modeling

The system under investigation comprises three main components: the partly superconducting synchronous generator, the power converter, and the control unit. A structured modeling workflow is adopted to accurately represent the coupled drivetrain system and its highly non-linear dynamics. The entire system model is implemented on a rapid prototyping platform based on the AMD Zynq 7030 System-on-Chip (SoC) to achieve real-time capability.

A. Electrically Excited Synchronous Generator Model

The use of high-temperature superconducting (HTS) windings for the field coils in the rotor of the generator allows for extremely high field excitation, resulting in iron saturation. Therefore, the model of the electrically excited synchronous machine is a highly non-linear, flux-based model implemented in the rotor-oriented d-q coordinate system. The flux linkages are determined from 2D Finite-Element Analysis (FEA), explained in detail in [1], and stored in multi-dimensional lookup tables, which are illustrated in Fig. 2. This approach is necessary to capture the effects of magnetic saturation [4]. The voltage equations for the stator windings are therefore given by:

$$v_{\mathrm{sd}} = R_{\mathrm{s}} \cdot i_{\mathrm{sd}} + \frac{\mathrm{d}\,\Psi_{\mathrm{sd}}}{\mathrm{d}t} - p \cdot \omega_{\mathrm{mech}} \cdot \Psi_{\mathrm{sq}} \tag{1}$$

$$v_{\mathrm{sq}} = R_{\mathrm{s}} \cdot i_{\mathrm{sq}} + \frac{\mathrm{d}\,\Psi_{\mathrm{sq}}}{\mathrm{d}t} + p \cdot \omega_{\mathrm{mech}} \cdot \Psi_{\mathrm{sd}} \tag{2}$$

The flux linkages Ψ_{sd} and Ψ_{sq} are functions of the currents i_{sd}, i_{sq} and the field winding current i_{rf}, e.g. $\Psi_{\mathrm{sd}} = f(i_{\mathrm{sd}}, i_{\mathrm{sq}}, i_{\mathrm{rf}})$. The ohmic stator resistance is represented by R_{s}, number of pole pairs by p and the mechanical angular speed by ω_{mech}. The field winding voltage equation is:

$$v_{\mathrm{rf}} = R_{\mathrm{r}} \cdot i_{\mathrm{rf}} + \frac{\mathrm{d}\,\Psi_{\mathrm{rf}}}{\mathrm{d}t} \tag{3}$$

where v_{rf} and i_{rf} are the field voltage and current, R_{r} is the rotor winding resistance, and Ψ_{rf} is the field winding flux linkage. The torque equation for the machine is given by:

$$T_{\mathrm{mech}} = \frac{3}{2} \cdot p \cdot (\Psi_{\mathrm{sd}} \cdot i_{\mathrm{sq}} - \Psi_{\mathrm{sq}} \cdot i_{\mathrm{sd}}) \tag{4}$$

The described machine model is implemented in the CHiL model using the inverse of the flux-linkage maps derived from FEA and represented by lookup tables (LUT) in Fig. 4. This enables accurate real-time emulation as it bridges the gap between conventional linear models and computationally intensive FEA simulations of this partly superconducting machine.

B. Power Converter and Drivetrain Model

The generator is connected to a conventional two-level voltage source power converter that feeds the three-phase stator winding. The converter is modeled by three switched voltage sources, with its switching states determined by the gate signals generated in the controller hardware and the calculated voltage of the DC link. For a more detailed analysis, a future power-hardware-in-the-loop (PHiL) setup will include a scaled-down hardware converter, accounting for real converter power losses including transient switching effects. Furthermore, the drivetrain includes a planetary gearbox for the mechanical interface between the generator shaft and turbine hub. The general structure of the CHiL setup for the coupled drivetrain system is shown in Fig. 1.

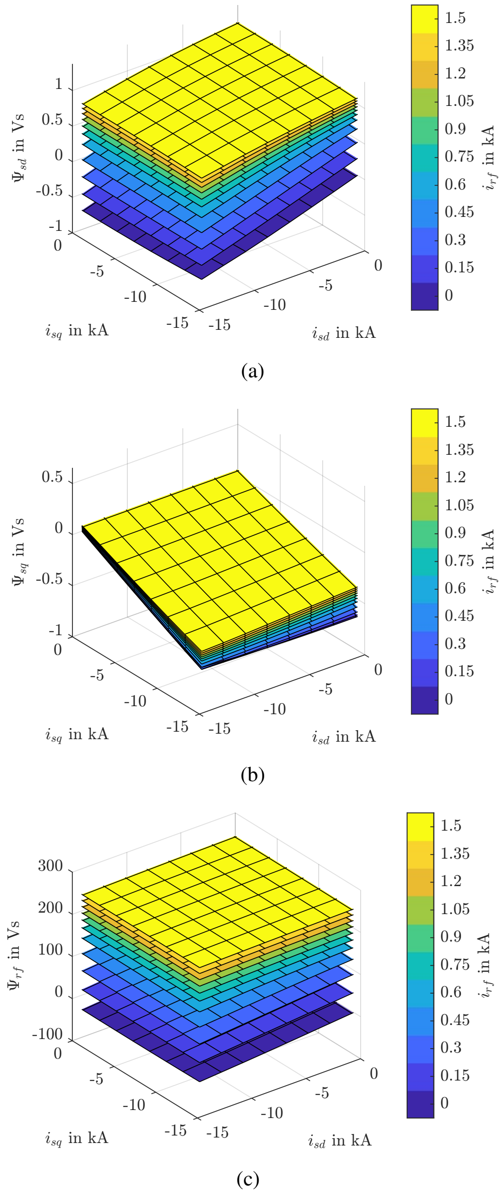

Fig. 2. Flux linkage maps of the stator d-axes Ψ_{sd} (a) and q-axes Ψ_{sq} (b), and rotor flux linkage Ψ_{rf} (c), resulting from FEA model for discrete excitation current values i_{rf}

C. Controller-Hardware-in-the-Loop Setup

The CHiL test bench is based on the Field-Programmable Gate Array (FPGA) inside the SoC. The drivetrain emulation-FPGA features a massively parallel architecture with 125 000 logic cells and high clock speed of 100 MHz in this application, which is essential for solving the equations of the machine model within the small time steps required for real-time simulation of high-order stator current harmonics greater than the converter switching frequency. Furthermore, the system features a block RAM of 9.3 Mb capable of storing

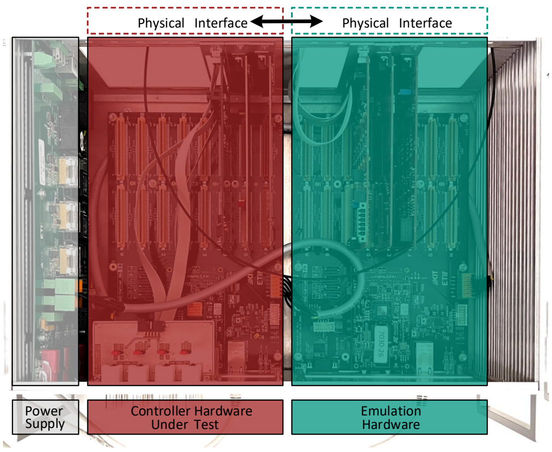

Fig. 3. CHiL hardware setup with two identical AMD Zynq 7030 SoC and respective peripheral hardware for controller hardware testing (left) and sensor emulation (right)

detailed inverse flux-linkage maps in the form of LUTs. The physical controller hardware under test (CHuT) is a digital signal processor connected to the emulation-FPGA via real-time interfaces in the form of hardware expansion cards for the SoC designed for sensor emulation.

The process can be explained as follows:

1) The emulation-FPGA receives control signals (e.g. switching states) from the physical CHuT with a control frequency of 2.5 kHz in the presented application.
2) The FPGA solves the converter model with 100 MHz and the machine model with 2 MHz to emulate quasi-continuous signals for the CHuT.
3) The emulation-FPGA outputs emulated sensor signals for all currents, voltages and the rotor position to the physical CHuT via SoC expansion cards.
4) The CHuT processes these signals, executes its control algorithm (e.g. field-oriented control) with 2.5 kHz and sends new control signals back to the emulation FPGA.

This continuous loop allows for the emulation of the physical system dynamics. The presented FPGA-based system offers the necessary computational power and low latency in order to enable the emulation of stator current harmonics with multiples of the converter switching frequency. A schematic of the CHiL model is shown in Fig. 4.

D. Hardware Under Test

The control of the superconducting generator is achieved using a standard Field-Oriented Control (FOC) scheme implemented on the Arm Cortex A9 processor of the CHuT. The FOC relies on accurate rotor position and speed information, which is provided by the real-time simulation in the CHiL setup with according sensor data emulated using a SoC expansion card. The output of the FOC is then transformed back to the stationary frame to generate the three-phase voltage references for the hardware modulation stage located on a dedicated SoC expansion card of the CHuT.

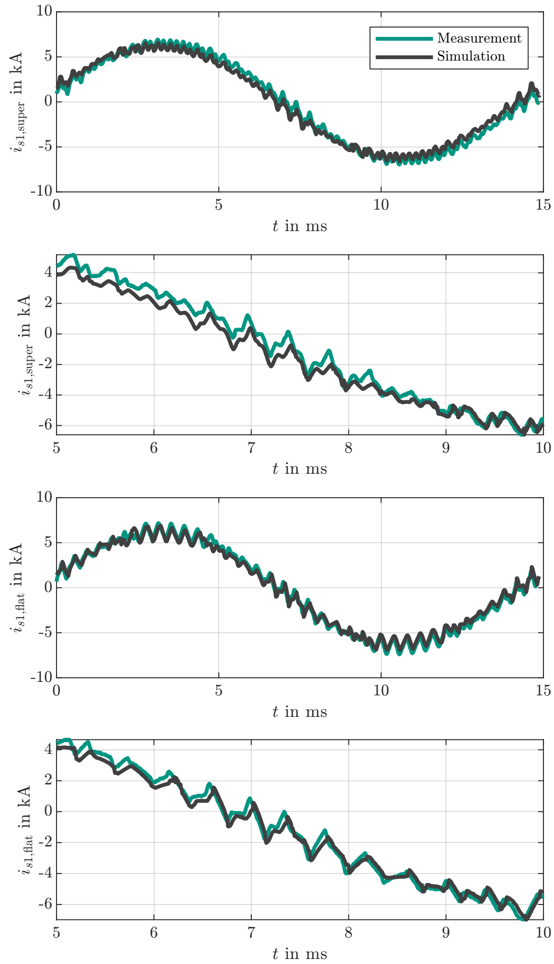

Fig. 5. Comparison of current waveforms for converter feeding with super-sine (top) and flat-top (bottom) modulation, both at a switching frequency of $f_\mathrm{s} = 2.5$ kHz, in simulation and measurement with the CHiL setup

III. Test Scenarios and Results

To investigate the system, CHiL was used to simulate two exemplary operating scenarios determined by the CHuT:

a) Super-Sine Modulation: The generator model is fed with pulsed voltages determined by the power converter model featuring an increased degree of modulation compared to a standard sine-triangle modulation.

b) Flat-Top Modulation: The generator model is fed with pulsed voltages featuring an increased harmonic content but reduced converter switching losses.

The simulations and hardware tests with the CHiL setup were performed across a range of operating points (varying speed and torque) with an exemplary current waveform at $n = 340$ rpm and $T = -110$ kNm illustrated in Fig. 5.

As seen in Fig. 5, the expected generator currents from the simulation model could be approximately replicated in real-time on a FPGA with the flux-linkage based modeling approach shown in Fig. 4.

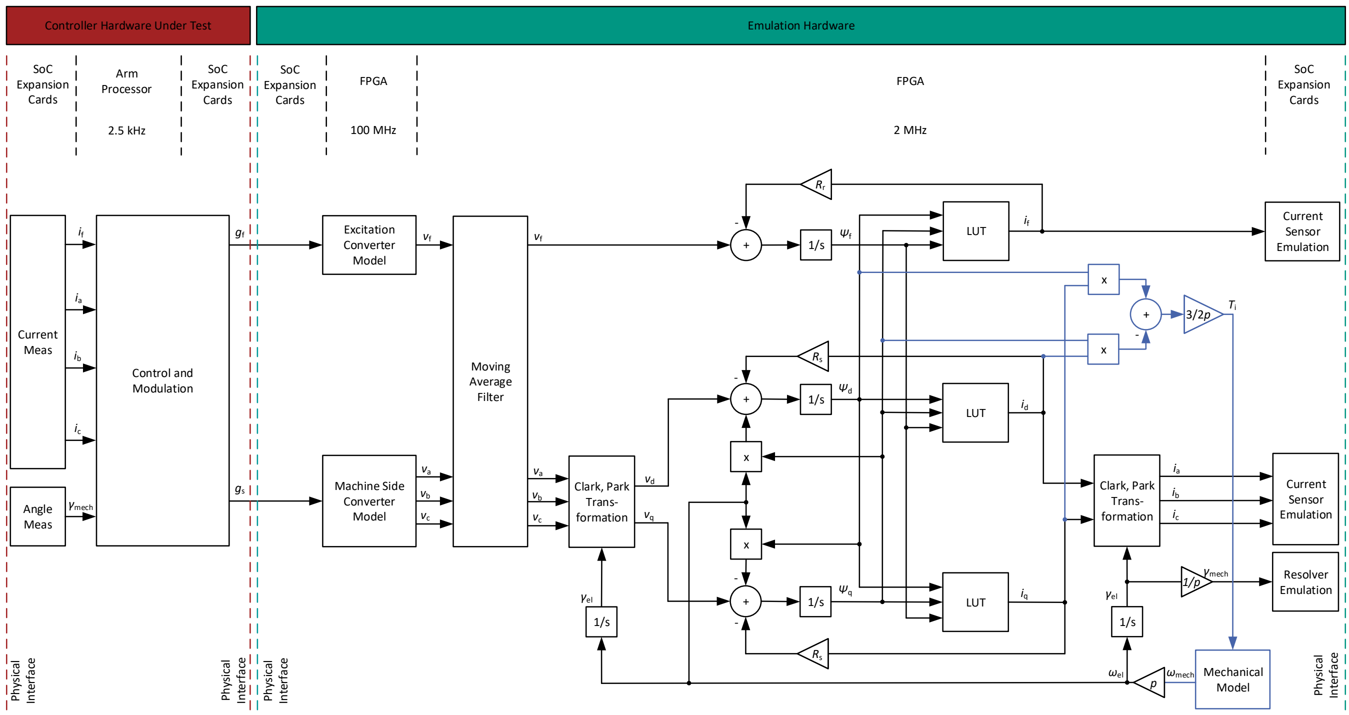

Fig. 4. Detailed schematic of the CHiL machine emulation, illustrating the real-time implementation of the flux-linkage based model on the FPGA (time-continuous representations in the figure for reasons of simplicity)

IV. Mechanism of Rotor Eddy Current Losses from Pulsed-Voltage Stator Feeding

A critical aspect of a superconducting machine design is the management of losses, particularly those occurring in the cryogenic components of the rotor. While the superconducting winding itself has zero DC resistance, losses can be induced in the surrounding normal-conducting structures. Due to power converter feeding, with pulsed voltage and non-sinusoidal current waveforms, eddy current losses in normal-conducting parts dominate the overall rotor losses and therefore the heat-load on the air-gap and the cryocooler.

The modulation scheme of the power converter results in voltage harmonics at multiples of the switching frequency. These harmonics create higher-order magnetic field waves that rotate at different speeds relative to the fundamental magnetic field. As these field waves pass through the rotating cryostat wall, acting as a damper screen, and the cryogenic parts or the rotor, they induce eddy currents in any conductive material.

In a first approximation, the total power P_{eddy} dissipated as heat due to eddy currents inside an electrically conductive damper screen on the rotor surface can be estimated using the following equation for an effective frequency f_{eff} of non-sinusoidal waveforms derived in [5]. From the transient single phase stator current $i_{\text{s}}(t)$, the time-dependent air-gap flux density $B_{\text{s}\delta}(t)$ can be estimated using the magnetic permeability μ, the width of the air-gap δ and the number of turns in the stator winding N.

$$B_{\text{s}\delta}(t) = \frac{\mu \cdot N}{2 \cdot \delta} \cdot i_{\text{s}}(t). \tag{5}$$

Since the damper screen is mounted on the rotor surface, the magnetic air-gap flux density $B_{\text{s}\delta}(t)$ obtained from the stator current in the stationary reference frame is transformed into the rotary reference frame $B_{\text{r}\delta}(t)$. The effective frequency f_{eff} of the non-sinusoidal magnetic flux-density is defined as follows.

$$f_{\text{eff}} = \frac{\sqrt{\frac{1}{T}\int_0^T \left(\frac{\mathrm{d}B_{\text{r}\delta}(t)}{\mathrm{d}t}\right)^2 \mathrm{d}t}}{2\pi \cdot \sqrt{\frac{1}{T}\int_0^T B_{\text{r}\delta}^2(t)\,\mathrm{d}t}} \tag{6}$$

Therefore, an effective skin depth δ_{skin} for the magnetic field inside of the damper screen with a thickness d_{screen} can be estimated in dependence of the specific electrical conductivity σ_{el}.

$$\delta_{\text{skin}} = \min\left[\sqrt{\frac{2}{\mu \cdot \sigma_{\text{el}} \cdot 2 \cdot \pi \cdot f_{\text{eff}}}},\ \text{d}_{\text{screen}}\right] \tag{7}$$

A geometry-dependent correction factor k_{geom} is introduced, which will converge to 1 for thin sheets with a large surface area A_{surface}.

$$k_{\text{geom}} = \frac{A_{\text{surface}}}{\delta_{\text{skin}}^2 + A_{\text{surface}}} \tag{8}$$

The proportionality factor k_{eddy}, which describes the eddy-current loss inside the damper screen, can be calculated as follows.

$$k_{\text{eddy}} = \frac{1}{12} \cdot \sigma_{\text{el}} \cdot \delta_{\text{skin}}^3 \cdot A_{\text{surface}} \cdot k_{\text{geom}} \tag{9}$$

Finally, the total power dissipated by the eddy currents in the sheet P_{eddy} inside a machine with a number of poles $2p$ and three symmetrical phases can be calculated.

$$P_{\text{eddy}} = k_{\text{eddy}} \cdot 2p \cdot 3 \cdot \frac{1}{T} \int_0^T \left(\frac{\mathrm{d}B_{\text{r}\delta}(t)}{\mathrm{d}t} \right)^2 \mathrm{d}t \tag{10}$$

In order to obtain the simplified formulation often found in literature, a single sinusoidal stator current harmonic of order ν with a frequency ${}^{\nu}f$ and an amplitude of the magnetic air-gap flux density ${}^{\nu}\hat{B}_{\delta}$ through a thin conductive damper screen on the surface of the rotor can be assumed.

Under these assumptions, the time derivative of the magnetic flux density exhibits a purely sinusoidal behavior, and the mean square value over one electrical period T is

$$\frac{1}{T} \int_0^T \left(\frac{\mathrm{d}^{\nu} B_{\text{r}\delta}(t)}{\mathrm{d}t} \right)^2 \mathrm{d}t = 2 \cdot \pi^2 \cdot {}^{\nu}f^2 \cdot \hat{B}_{\text{r}\delta}^2 \tag{11}$$

Consequently, the squared RMS value of the time derivative of the magnetic flux density appearing in (10) may be replaced by an explicit expression in terms of the harmonic frequency and amplitude. This yields the well-known closed-form expression for the eddy-current losses associated with the νth harmonic

$${}^{\nu}P_{\text{eddy}} = 2p \cdot 3 \cdot \frac{\pi^2 \cdot {}^{\nu}\hat{B}_{\text{r}\delta}^{\;2} \cdot \delta_{\text{skin}}^3({}^{\nu}f) \cdot \sigma_{\text{el}} \cdot {}^{\nu}f^2}{6} \cdot A_{\text{surface}} \tag{12}$$

The same modeling approach can be applied to estimate the eddy-current losses inside rotor components located beneath the damper screen, such as the normal-conducting pole core. In this case, the magnetic flux density on the surface of the pole core $B_{\text{pole}}(t)$ can be approximated by an exponential decay of the air-gap flux density $B_{\text{r}\delta}(t)$ across the damper screen thickness d_{screen}.

$$B_{\text{rpole}}(t) = (B_{\text{r}\delta}(t)) \cdot e^{-\dfrac{d_{\text{screen}}}{\delta_{\text{skin}}}} \tag{13}$$

Here, δ_{skin} denotes the effective skin depth of the magnetic field inside the damper screen as defined previously. The time-dependent flux density $B_{\text{rpole}}(t)$ may then be used analogously to $B_{\text{r}\delta}(t)$ in the definition of the effective frequency and the subsequent eddy-current loss calculation for the pole core.

In order to validate the approach, a simple transient finite element analysis (FEA) of the three-phase 5/6-pitched machine, featuring the mechanical specifications given in Tab. I, is carried out in a highly saturated operating point. Therefore $\mu = \mu_0$ can be assumed for the analytical calculations. Resulting eddy-current losses ${}^{\nu}P_{\text{eddy}}$ for individual stator current harmonic of an representative amplitude $\hat{i}_{\text{s}} = 200\,\text{A}$ and order $\nu \in [2, 42]$ are illustrated in Fig. 6 for the analytical approach presented in this section and for FEA simulations.

TABLE I
GEOMETRICAL SPECIFICATIONS OF THE GENERATOR

Number of stator turns	N	2
Number of poles	$2p$	24
Effective magnetic air-gap	δ	35 mm
Thickness of the damper screen	d_{screen}	10 mm
Pitch of the pole	τ_{pole}	190 mm
Width of the rotor pole core	w_{pole}	90 mm
Length of the active iron	l_{Fe}	320 mm

The eddy-current losses dissipated in the normal-conducting cryogenic pole core in Fig. 6 are evaluated with respect to the required electrical cooling power by considering a coefficient of performance (COP) of 1.3%, corresponding to a state-of-the-art Gifford–McMahon cryocooler [6]. This emphasizes sufficient damper screen design and careful material selection regarding the material properties mentioned above.

In order to visualize the spatial electromagnetic state of the machine, a transient FEA is performed. Fig. 7 illustrates the spatial distribution of the magnetic flux density norm $|B|$ at an exemplary time step t_0. The observed induction patterns, particularly the penetration of harmonic field waves into the damper screen, align with theoretical expectations and the results exhibit high consistency with investigations like [7].

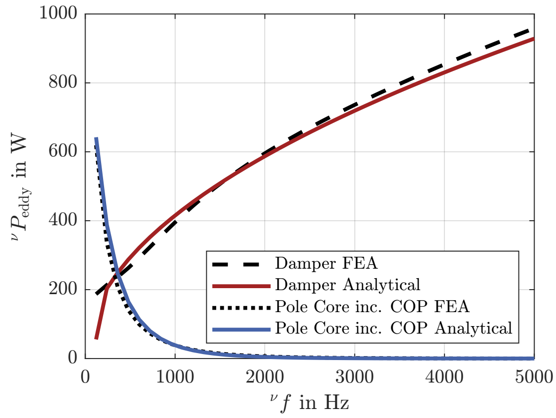

Fig. 6. Comparison of the total power dissipated by eddy currents in the damper screen and pole core using analytical calculations and FEA at $\hat{i}_{\text{s}} = 200\,\text{A}$ and $\nu \in [2, 42]$

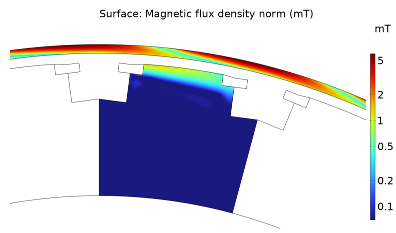

Fig. 7. FEA of magnetic flux density $|B|(t_0)$ inside the rotor for a single stator current harmonic of frequency ${}^{\nu}f = 240\,\text{Hz}$ and amplitude $\hat{i}_s = 200\,\text{A}$

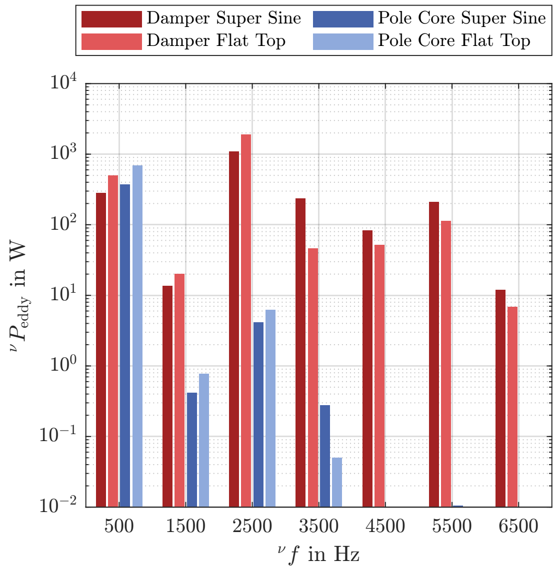

Fig. 8. Comparison of eddy-current loss in the damper screen and pole core including COP for converter feeding with super-sine and flat-top modulation

V. Rotor Eddy Current Losses Depending on the Modulation of the Power Converter

The resulting thermal loads on the ventilation of the air-gap and the cryogenic cooling system are investigated for power converter feeding of the medium-speed wind turbine generator at nominal rotational speed $n = 600\,\text{rpm}$ and nominal torque $T = -200\,\text{kNm}$. The spectral distribution of these losses is presented in Fig. 8, comparing super-sine and flat-top modulation strategies respective current spectra at a constant switching frequency of $f_{\text{s}} = 2.5\,\text{kHz}$.

To evaluate the impact of the stator current harmonics, the spectral power loss due to eddy-currents was calculated from the high-fidelity 2 MHz machine model and subsequently accumulated into bins of 1 kHz for illustrative purposes. The analysis of the damper eddy current losses over the full frequency spectrum reveals a dominant peak at the 2.5 kHz switching frequency. Due to the effective design of the damper screen, no significant eddy current losses inside the cryogenic pole core are observed in the frequency bins at or above the switching frequency f_s. However, the influence of the chosen modulation strategy is clearly visible in the magnitude of losses inside the damper screen at $^{\nu}f \geq f_s$. Specifically, for the losses in the damper screen at the switching frequency, an increase of approximately 75% is observed when utilizing flat-top modulation compared to super-sine modulation. This increase is attributed to the higher harmonic content inherent in the flat-top approach.

Furthermore, the results indicate increased eddy current losses in the cryogenic pole core for harmonic frequencies below 1 kHz. This represents a critical design constraint for the total cryogenic cooling system, as heat removal at cryogenic temperatures is extremely power-intensive. The magnitude of these low-frequency losses directly impacts the specifications for the cooling bus at approximately 30 K, the required number of cold heads, and the overall cryo-compressor power needed to maintain the superconducting state of the field windings.

VI. Conclusion and Outlook

The CHiL investigations of the partly superconducting wind turbine generator prototype provided key insights into drive-train dynamics. Using a high-fidelity, real-time simulation platform, it has been confirmed that coupled modeling of the generator and its power converter is essential for the prediction of converter-induced thermal loads on the generator rotor. Converter-induced harmonic field waves lead to a substantial increase in rotor eddy current losses inside the damper and within the cryogenic rotor parts, posing a significant challenge to the cryogenic cooling system. This finding validates the focus on the development of advanced modulation schemes to reduce these losses and to test the appropriate control hardware. Therefore, power converter modulation not only regulates the generator output power but also actively reduces the harmonic content of the stator currents, thereby reducing the thermal load on the cryogenic rotor and improving the overall system efficiency. The CHiL test bench serves as a crucial tool for the hardware implementation of future control strategies for the megawatt-scale prototype.

Acknowledgments

The authors acknowledge the financial support of this work by the German Federal Ministry for Economic Affairs and Energy. (03EE3094C)

References

[1] N. Thönelt, R. Köster, M. Hiller, Y. Burkhardt and A. Binder, "Coupled Generator- and Converter-Modelling for Partly Superconducting Medium-Speed Wind Turbine Generators," in Conference on Sustainable Energy Supply and Energy Storage Systems (NEIS) 2025, doi:10.30420/566633023.

[2] T. Arndt, M. Eisele, M. Kläser, A. Binder, R. Köster, A. Jöckel, R. Zeichfüßl and J. Krämer, "Speedy_HTS – An HTS Rotor for an Uprated Mid-Speed Wind Power Generator," in IEEE Transactions on Applied Superconductivity, vol. 36, no. 3, pp. 1-4, May 2026, Art no. 5200104, doi: 10.1109/TASC.2025.3619467.

[3] T. Hardy and W. Jewell, "Hardware-in-the-Loop Wind Turbine Simulation Platform for a Laboratory Feeder Model," in IEEE Transactions on Sustainable Energy, vol. 5, no. 3, pp. 1003-1009, July 2014, doi: 10.1109/TSTE.2014.2320600.

[4] P. Winzer, J. Richter and M. Doppelbauer, "Dynamic control of generalized electrically excited synchronous machines using predictive flux control", Florence, Italy, 2016, pp. 2772-2777, doi: 10.5445/IR/1000066763

[5] J. Li, T. Abdallah and C. R. Sullivan, "Improved calculation of core loss with nonsinusoidal waveforms," Conference Record of the 2001 IEEE Industry Applications Conference. 36th IAS Annual Meeting (Cat. No.01CH37248), Chicago, IL, USA, 2001, pp. 2203-2210 vol.4, doi: 10.1109/IAS.2001.955931.

[6] Technical Specification "AL325 Gifford-McMahon Cryocooler", Bluefors Cryocooler Technologies Inc., 2024.

[7] M. Nakano, H. Kometani and M. Kawamura, "A study on eddy-current losses in rotors of surface permanent-magnet synchronous machines," in IEEE Transactions on Industry Applications, vol. 42, no. 2, pp. 429-435, March-April 2006, doi: 10.1109/TIA.2006.870037.